The isobaric tags for relative and absolute quantification-based quantitative proteomics of fresh tissue-derived secretome in hepatocellular carcinoma

Hai-Tao Jiang[1,2,3], Guo-Sheng Gao[2,3,4], Feng Ren[1,2,3], Yun-Jie Chen[1,2,3]*

[1]Department of General Surgery, HwaMei Hospital, University of Chinese Academy of Sciences, China
[2]Ningbo Institute of Life and Health Industry, University of Chinese Academy of Sciences, China
[3]Key Laboratory of Diagnosis and Treatment of Digestive System Tumors of Zhejiang Province, China
[4]Department of Clinical Laboratory, HwaMei Hospital, University of Chinese Academy of Sciences, China

***Corresponding author:**
Yun-Jie Chen
Department of General Surgery
HwaMei Hospital
University of Chinese Academy of Sciences
China
E-mail: yunjiechen1216@163.com

Submitted: 11 December 2019; **Accepted:** 10 March 2020
Online publication: 3 February 2021

Arch Med Sci 2025; 21 (4): 1536–1555
DOI: https://doi.org/10.5114/aoms/118871

Abstract

Introduction: Proteomics technology platforms offer an extremely useful tool for the discovery of new cancer biomarkers. Secreted proteins play important roles in signal transduction, cellular growth, proliferation, differentiation, and apoptosis. This study aimed to investigate the molecular signatures of the hepatocellular carcinoma (HCC) by quantitative proteomics using isobaric tags for relative and absolute quantification (iTRAQ) with liquid chromatography-tandem mass spectrometry (LC-MS/MS).

Material and methods: In this study, we used an iTRAQ-based quantitative proteomic approach to analyse the secretome of HCC tissues to identify plasma biomarkers. Serum-free conditioned media (CM) were collected from the primary cultures of cancerous tissues, the surrounding noncancerous tissues, and distal noncancerous tissues.

Results: A proteomic analysis of the CM proteins allowed for a total of 5214 identified proteins, of which 190 and 44 proteins were dysregulated in the HCC tissues/distal noncancerous tissues (HCC/DN group) and the adjacent noncancerous tissues/distal noncancerous tissues (AN/DN group) compared with the distal noncancerous tissues. The dysregulated proteins in the HCC/DN group were concentrated in mitogen-activated protein kinase (MAPK) signalling and Janus kinase-signal transducer and activator of the transcription (JAK-STAT) signalling, but the dysregulated proteins in the AN/DN group were more concentrated in the basal material metabolism.

Conclusions: The secretome profile alternations and signalling pathways were associated with HCC incidence and development. The dysregulated proteins in the HCC/DN group were concentrated in the MAPK signalling and JAK-STAT signalling, but the dysregulated proteins in the AN/DN group were more concentrated in the basal material metabolism.

Key words: hepatocellular carcinoma, isobaric tags for relative and absolute quantification, tissue secretome, incidence and development, molecular mechanism.

Introduction

Hepatocellular carcinoma (HCC) is a kind of clinical common malignant tumour with an insidious onset, which is invasively fast-growing

and has a poor prognosis [1]. Although surgical excision was demonstrated to be the first choice for HCC treatment, most HCC is not diagnosed until the advanced stage of the disease, when surgical treatments are not suitable for treating the disease [2]. Therefore, early detection and treatment are key to improving therapeutic outcomes, reducing mortality, and increasing the long-term survival rate in HCC patients.

Alpha-fetoprotein (AFP) was the only widely accepted and applied biomarker in clinical practice because of its practical value for the diagnosis and monitoring of the development of HCC. However, the AFP method experienced insufficient sensitivity and specificity in the early diagnosis of HCC. Meanwhile, the AFP level is also easily affected by other diseases, such as hepatitis during pregnancy and liver regeneration after damage, which increases the inaccuracy of clinical diagnoses [3–5]. There is, therefore, an urgent need to identify new biomarkers with high sensitivity and high specificity for the early diagnosis of HCC.

Proteomics technology platforms are an extremely useful tool for the discovery of new cancer biomarkers. A highly desirable biomarker for cancer screening and monitoring would be a biomarker that can be measured in body fluid samples [6]. Accordingly, blood samples such as serum and plasma have been the ideal targets of proteomics studies aimed at identifying cancer diagnostic and prognostic biomarkers [7, 8]. However, several challenges have hindered the progress of these studies. The main 2 reasons include the complex nature of serum and plasma samples and the large dynamic range between the concentrations of different proteins.

Secreted proteins play important roles in signal transduction, cellular growth, proliferation, differentiation, and apoptosis. They are also important in tumourigenesis, development, invasion, and metastasis of HCC [9]. Therefore, the secretomes of cell lines are also performed during screening. Many researchers have reported the application of secretomes in the screening of diagnostic and prognostic protein biomarkers [10–12]. Essentially, it is well established that any potential biomarker candidates screened from HCC cell lines should be ultimately validated in clinical tissue samples that are closer to tumours than any of the model systems. As a result, it is more direct and convincing to utilise the primary culture of tumour tissues and the proteomic analysis of serum-free conditioned media to search the diagnostic or prognostic biomarkers [13, 14].

We, thus, conducted this study to investigate the molecular signatures of HCC by quantitative proteomics using isobaric tags for relative and absolute quantification (iTRAQ) coupling with liquid chromatography-tandem mass spectrometry (LC-MS/MS).

Material and methods

Sample collection and tissue culture *in vitro*

In our study, the HCC tissue group, the adjacent noncancerous tissue (AN) group, and the distal noncancerous tissue (DN) group were obtained from 2 primary HCC patients who were diagnosed with HCC by post-operative pathological examinations and subjected to standard radical resection. The fresh tissues were collected at the time of surgery from the HCC patients and immediately washed with phosphate-buffered saline in a sterile environment. Subsequently, the tissues were cut into 2 mm^3 pieces, washed several times until the tissues became colourless, and then cultured in a Dulbecco's modified eagle serum-free medium at 5% CO_2 for 24 h. Thereafter, the supernatants were collected for protein extraction. This study was approved by the Ethics Committee of our hospital, and the 2 patients signed informed consent forms.

Protein extraction and digestion

The collected culture supernatant was centrifuged at a low speed (200 g) to remove the cells and tissue debris and then filtered with a 0.22 µm filter membrane to remove the residual cells. Thereafter, the filtrate was concentrated with 3K ultrafiltration until the phenolic red colour was completely removed. The proteins were precipitated by ice-cold acetone, and the protein concentration of the supernatant was determined by bicinchoninic acid assay following the manufacturer's protocol. Subsequently, 4 µl of a reducing reagent was added to each sample tube and vortex to mix and incubate the tubes at 60°C for 1 h, and 2 µl of a cysteine blocking reagent was added to each tube and vortex to mix and incubate the tubes at room temperature for 10 min. Finally, the proteins were digested by sequence-grade modified trypsin through filter-aided sample preparation.

Isobaric tags for relative and absolute quantification labelling

The peptides from 100 µg proteins per group were labelled according to the Applied Biosystems iTRAQ™ reagent chemistry reference guide. The peptides were labelled as follows: 2 HCC groups were labelled 113 and 114, 2 AN groups were labelled 114 and 115, 2 DN groups were labelled 116 and 117, and the mixed DN group samples with an equal amount were labelled 119 and 121. The labeled peptides were mixed with an equal amount and dried in a vacuum centrifuge for further usage.

High pH reversed-phase separation

The dried peptide mixture was fractionated by high pH separation using ekspert™ ultraLC 100

pump. Mobile phase A: 20 mM ammonium formate in water, mobile phase B: 20 mM ammonium formate in 80% ACN, the pH was adjusted to 10.0 with ammonium hydroxide. High pH (pH = 10) separation was performed using a 65-min linear gradient as follows: 0–5 min, 0–5% B; 5–30 min, 5–15% B; 30–45 min, 15–38% B; 45–46 min, 38–90% B, 46–54.5 min, 90–90% B; 54.5–55 min, 90–5% B; 55–65 min, 5–5% B. Finally, 40 fractions were collected, and 4 fractions with the same time interval were pooled together to reduce the fraction numbers, such as 1, 2 and 21, 22 and 3, 4 and 23, 24, and so on [15]. Ten fractions at the end were dried in a vacuum concentrator for further usage.

The Nano-LC-MS/MS analysis

The fractions were re-suspended with 30 µl solution A (solution A: 0.1% FA and 2% ACN in water) and 8 µl was loaded on an exigent nano LC-Ultra™ system nano-LC with a trap column (ChromXP C18-CL-3 µm, 120A, 350 µm × 0.5 µm) with a flow of 2 µl/min. The column flow rate was maintained at 300 nl/min with a 101 min linear gradient as follows: 0–0.1 min, 5–10% B; 0.1–60 min, 10–25% B; 60–85 min, 25–48% B; 85–86 min, 48–80% B, 86–90 min, 80–80% B; 90–91 min, 80–5% B; 91–101 min, 5–5% B (solution B: 0.1% FA and 2% ACN in water). The MS data were collected by the Triple TOF 5600 system. The electrospray voltage of 2.3 kV and 150°C heating at the inlet of the mass spectrometer was used. The resolution was set at 30,000 with the scan range of 300–1500 m/z. The cumulative scanning time was 250 ms in the high-resolution scanning mode, and up to 40 sub-ion scans could be performed each time. Each Fraction was repeated three times with instrumental analysis, and all parent ions were collision-induced dissociation using fluctuating collision energy.

Data analysis

The MS data were processed using ProteinPilot 4.5 (AB SCIX, Foster City, CA, USA) and then searched using Mascot (version 2.2; Matrix Science, London, United Kingdom) search algorithms against the UniProt human database. The enzyme specificity of trypsin was used and up to a maximum of 2 missed cleavages were allowed for protease digestion. Mascot was searched with a parent ion tolerance of 10 parts per million (ppm) and a fragment ion mass tolerance of 0.05 Da. Carbamidomethylation of cysteine, as well as iTRAQ modification of peptide N-terminus and lysine residues, were set as a fixed modification; oxidation of methionine and iTRAQ 8-plex labelling of tyrosine were specified as variable modifications. The proteins were accepted if the protein FDR was < 1%. To identify proteins whose expression was significantly altered in the 2 different groups, a threshold of the iTRAQ ratios were used to define differentially expressed proteins. The proteins were considered to be differentially expressed if the iTRAQ ratio was > 1.5 or < 0.67 in the 2 different groups with the *p*-value of < 0.05, which were statistically analysed by a paired *T*-test. The gene ontology (GO) annotation and pathway enrichment analysis of the differentially expressed proteins were carried out using the online tool DAVID (http://david.abcc.ncifcrf.gov/). The gene ontology annotation contains biological processes, cell components, and molecular functions. The pathway analysis was based on the Kyoto Encyclopaedia of Genes and Genomes (KEGG) database. The gene ontology annotations and signalling pathways were ranked in terms of the enrichment or number of the differentially expressed proteins. The protein and protein interaction was performed using the online String database (https://string-db.org/).

Results

The relative quantification of the secretome of the primary hepatocellular carcinoma patients

In this study, total proteins were extracted from the collected tumours, their adjacent noncancerous tissues and their distal noncancerous tissues were taken from patients and analysed using iTRAQ 2D LC-MS/MS, and the workflow as described in Figure 1. In total, we quantified 5214 proteins, of which 190 and 44 proteins were classified as differentially expressed in the HCC tissues/distal noncancerous tissues (HCC/DN) group and the adjacent noncancerous tissues/distal noncancerous tissues (AN/DN) group (Tables I and II). As is evident in Figure 2A, the number of differentially expressed proteins identified in the HCC/DN group was much higher than that in the AN/DN group.

When we compared the differences between the 2 groups, we found that among these differentially expressed proteins, 35 proteins altered their expression in both HCC types, while 155 proteins were dysregulated in the HCC/DN group only and 9 proteins were dysregulated in the AN/DN group only (Figure 2 B). We then analysed the biological functions and signalling pathways of these proteins, including the proteins differentially expressed in both groups and the proteins differentially expressed individually in 1 group.

The gene ontology analysis of the differentially expressed proteins in primary hepatocellular carcinomas

The gene ontology annotation analysis showed that the cell components of the differentially ex-

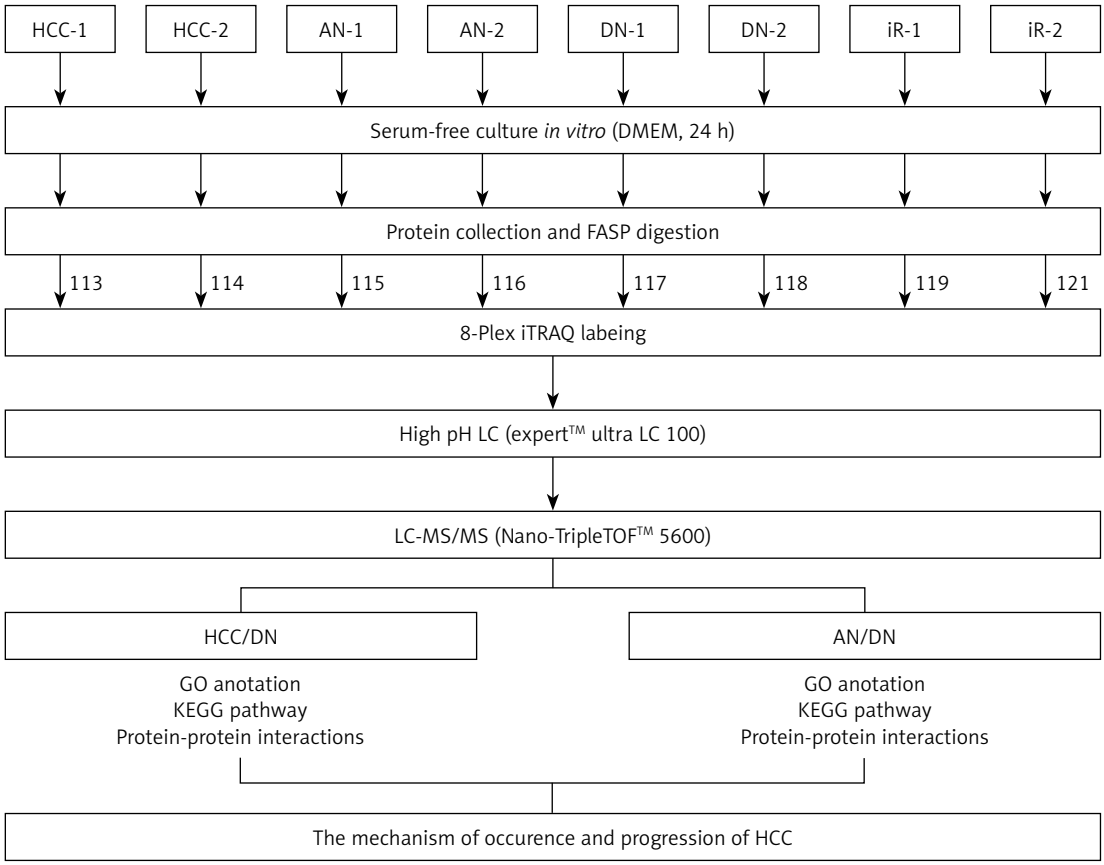

Figure 1. A schematic view of the experimental design and the isobaric tags for relative and absolute quantification (iTRAQ) 8 plex-labelling. Sample preparation procedures for shotgun mass spectrometry (MS/MS) analysis and important steps in the proteomic strategies were included. The tissues from the primary hepatocellular carcinoma (HCC) patients were divided into 3 groups: HCC group, adjacent noncancerous group, and dendritic cell group. Different tissues were cultured in a serum-free medium and the proteins were extracted from the cultural supernatant and then digested by trypsin and labelled by different iTRAQ reagents. The digested peptides were separated by high pH reversed-phase liquid chromatography (LC) and analysed by LC-MS/MS

pressed proteins either overlapped in the 2 groups or were unique in 1 group and were mostly located in the extracellular exosome (Figure 3). For the biological process analysis, the GO annotation analysis showed that the proteins overlapped in both groups and were the major participants in the protein folding, lipid metabolic process, gluconeogenesis, nucleobase-containing compound metabolic process, and canonical glycolysis (Figure 3 A).

There were 155 dysregulated proteins in the HCC group compared to the distal noncancerous tissues (DN) group, but these proteins were not dysregulated in the adjacent noncancerous (AN) tissues group compared to the DN group. These dysregulated proteins were mainly involved in signal transduction, cell proliferation, protein stabilisation, and negative regulation of the apoptotic process (Figure 3 B).

Interestingly, there were 9 dysregulated proteins in the AN group compared to the DN group, but they were not dysregulated in the HCC group compared to the DN group. The gene ontology results also showed that these dysregulated proteins were mainly involved in desmosome organisation, positive regulation of sister chromatid cohesion, translation, rRNA processing, nuclear-transcribed mRNA catabolic process, translational initiation, and SRP-dependent co-translational protein targeting to the membrane (Figure 3 C).

The Kyoto Encyclopaedia of Genes and Genomes pathway analysis of the differentially expressed proteins

As shown in Figure 4, the pathway of metabolism, genetic information processing, environmental information processing, and cellular was analysed. According to the results of the analysis, the dysregulated proteins in HCC are mostly involved in the Janus kinase-signal transducer and activator of the transcription (JAK-STAT) pathway and mitogen-activated protein kinase (MAPK) pathway. However, the signalling pathway that was only enriched in the AN group comprised mainly basic metabolisms, such as biological oxidations, amino

Table I. Differentially expressed proteins identified between hepatocellular carcinoma tissues and distal noncancerous tissues

No.	Accession	Name	FC	*P*-value
1	sp|P08670|VIME_HUMAN	Vimentin OS = Homo sapiens GN = VIM PE = 1 SV = 4	4.875285	0.00000000486
2	sp|P16615|AT2A2_HUMAN	Sarcoplasmic/endoplasmic reticulum calcium ATPase 2 OS = Homo sapiens GN = ATP2A2 PE = 1 SV = 1	4.655861	0.000000146
3	sp|P07602|SAP_HUMAN	Prosaposin OS = Homo sapiens GN = PSAP PE = 1 SV = 2	4.613176	0.00058
4	sp|P10809|CH60_HUMAN	60 kDa heat shock protein, mitochondrial OS = Homo sapiens GN = HSPD1 PE = 1 SV = 2	4.487454	0.0000000000382
5	sp|P14314|GLU2B_HUMAN	Glucosidase 2 subunit beta OS = Homo sapiens GN = PRKCSH PE = 1 SV = 2	3.872576	0.000281
6	sp|P31327|CPSM_HUMAN	Carbamoyl-phosphate synthase [ammonia], mitochondrial OS = Homo sapiens GN = CPS1 PE = 1 SV = 2	3.531832	0.0000000000162
7	sp|Q10471|GALT2_HUMAN	Polypeptide N-acetylgalactosaminyltransferase 2 OS = Homo sapiens GN = GALNT2 PE = 1 SV = 1	3.43558	0.00000579
8	sp|Q04695|K1C17_HUMAN	Keratin, type I cytoskeletal 17 OS = Homo sapiens GN = KRT17 PE = 1 SV = 2	3.311311	0.000898
9	sp|P05783|K1C18_HUMAN	Keratin, type I cytoskeletal 18 OS = Homo sapiens GN = KRT18 PE = 1 SV = 2	3.162278	0.0000367
10	sp|P32004|L1CAM_HUMAN	Neural cell adhesion molecule L1 OS = Homo sapiens GN = L1CAM PE = 1 SV = 2	3.133286	0.00000598
11	sp|P27797|CALR_HUMAN	Calreticulin OS = Homo sapiens GN = CALR PE = 1 SV = 1	3.076097	0.00000882
12	sp|P07237|PDIA1_HUMAN	Protein disulphide-isomerase OS = Homo sapiens GN = P4HB PE = 1 SV = 3	3.019952	0.000287
13	sp|P55084|ECHB_HUMAN	Trifunctional enzyme subunit beta, mitochondrial OS = Homo sapiens GN = HADHB PE = 1 SV = 3	2.85759	0.000323
14	sp|P80723|BASP1_HUMAN	Brain acid soluble protein 1 OS = Homo sapiens GN = BASP1 PE = 1 SV = 2	2.85759	0.0000445
15	sp|Q14697|GANAB_HUMAN	Neutral alpha-glucosidase AB OS = Homo sapiens GN = GANAB PE = 1 SV = 3	2.805434	0.00000569
16	sp|Q00839|HNRPU_HUMAN	Heterogeneous nuclear ribonucleoprotein U OS = Homo sapiens GN = HNRNPU PE = 1 SV = 6	2.728978	0.000519
17	sp|Q12931|TRAP1_HUMAN	Heat shock protein 75 kDa, mitochondrial OS = Homo sapiens GN = TRAP1 PE = 1SV = 3	2.679168	0.000193
18	sp|P14625|ENPL_HUMAN	Endoplasmin OS = Homo sapiens GN = HSP90B1 PE = 1 SV = 1	2.630268	0.0000362
19	sp|P40939|ECHA_HUMAN	Trifunctional enzyme subunit alpha, mitochondrial OS = Homo sapiens GN = HADHA PE = 1 SV = 2	2.630268	0.000143
20	sp|P27824|CALX_HUMAN	Calnexin OS = Homo sapiens GN = CANX PE = 1 SV = 2	2.630268	0.0000476
21	sp|P42704|LPPRC_HUMAN	Leucine-rich PPR motif-containing protein, mitochondrial OS = Homo sapiens GN = LRPPRC PE = 1 SV = 3	2.558586	0.0000000421
22	sp|P06576|ATPB_HUMAN	ATP synthase subunit beta, mitochondrial OS = Homo sapiens GN = ATP5B PE = 1 SV = 3	2.558586	0.00071
23	sp|Q8TEM1|PO210_HUMAN	Nuclear pore membrane glycoprotein 210 OS = Homo sapiens GN = NUP210 PE = 1 SV = 3	2.558586	0.000049
24	sp|P05023|AT1A1_HUMAN	Sodium/potassium-transporting ATPase subunit alpha-1 OS = Homo sapiens GN = ATP1A1 PE = 1 SV = 1	2.535129	0.000341
25	sp|P02545|LMNA_HUMAN	Prelamin-A/C OS = Homo sapiens GN = LMNA PE = 1 SV = 1	2.511886	0.000397
26	sp|Q9NR30|DDX21_HUMAN	Nucleolar RNA helicase 2 OS = Homo sapiens GN = DDX21 PE = 1 SV = 5	2.511886	0.000515
27	sp|P02786|TFR1_HUMAN	Transferrin receptor protein 1 OS = Homo sapiens GN = TFRC PE = 1 SV = 2	2.466039	0.000549
28	sp|P49792|RBP2_HUMAN	E3 SUMO-protein ligase RanBP2 OS = Homo sapiens GN = RANBP2 PE = 1 SV = 2	2.443431	0.000679

Table I. Cont.

No.	Accession	Name	FC	*P*-value
29	sp|Q86UP2|KTN1_HUMAN	Kinectin OS = Homo sapiens GN = KTN1 PE = 1 SV = 1	2.421029	0.000000491
30	sp|Q07065|CKAP4_HUMAN	Cytoskeleton-associated protein 4 OS = Homo sapiens GN = CKAP4 PE = 1 SV = 2	2.421029	0.00000087
31	sp|P11021|GRP78_HUMAN	78 kDa glucose-regulated protein OS = Homo sapiens GN = HSPA5 PE = 1 SV = 2	2.398833	0.0000000146
32	sp|Q9P2E9|RRBP1_HUMAN	Ribosome-binding protein 1 OS = Homo sapiens GN = RRBP1 PE = 1 SV = 4	2.398833	0.000000948
33	sp|P52272|HNRPM_HUMAN	Heterogeneous nuclear ribonucleoprotein M OS = Homo sapiens GN = HNRNPM PE = 1 SV = 3	2.208005	0.000000866
34	sp|P04843|RPN1_HUMAN	Dolichyl-diphosphooligosaccharide-protein glycosyltransferase subunit 1 OS = Homo sapiens GN = RPN1 PE = 1 SV = 1	2.208005	0.00056
35	sp|Q9UQ35|SRRM2_HUMAN	Serine/arginine repetitive matrix protein 2 OS = Homo sapiens GN = SRRM2 PE = 1 SV = 2	2.167704	0.0000419
36	sp|P08195|4F2_HUMAN	4F2 cell-surface antigen heavy chain OS = Homo sapiens GN = SLC3A2 PE = 1 SV = 3	2.108628	0.000497
37	sp|Q16891|MIC60_HUMAN	MICOS complex subunit MIC60 OS = Homo sapiens GN = IMMT PE = 1 SV = 1	2.108628	0.00000733
38	sp|Q96RP9|EFGM_HUMAN	Elongation factor G, mitochondrial OS = Homo sapiens GN = GFM1 PE = 1 SV = 2	2.108628	0.000905
39	sp|P78527|PRKDC_HUMAN	DNA-dependent protein kinase catalytic subunit OS = Homo sapiens GN = PRKDC PE = 1 SV = 3	2.089296	0.000000377
40	sp|Q9NSE4|SYIM_HUMAN	Isoleucine--tRNA ligase, mitochondrial OS = Homo sapiens GN = IARS2 PE = 1 SV = 2	2.070141	0.000341
41	sp|Q9H0D6|XRN2_HUMAN	5'-3' exoribonuclease 2 OS = Homo sapiens GN = XRN2 PE = 1 SV = 1	2.051162	0.000538
42	sp|Q9NZM1|MYOF_HUMAN	Myoferlin OS = Homo sapiens GN = MYOF PE = 1 SV = 1	2.013724	0.000021
43	sp|Q08211|DHX9_HUMAN	ATP-dependent RNA helicase A OS = Homo sapiens GN = DHX9 PE = 1 SV = 4	2.013724	0.000672
44	sp|P38646|GRP75_HUMAN	Stress-70 protein, mitochondrial OS = Homo sapiens GN = HSPA9 PE = 1 SV = 2	1.995262	0.00000556
45	sp|P25705|ATPA_HUMAN	ATP synthase subunit alpha, mitochondrial OS = Homo sapiens GN = ATP5A1 PE = 1 SV = 1	1.995262	0.0000861
46	sp|P13667|PDIA4_HUMAN	Protein disulphide-isomerase A4 OS = Homo sapiens GN = PDIA4 PE = 1 SV = 2	1.958845	0.00000668
47	sp|P06748|NPM_HUMAN	Nucleophosmin OS = Homo sapiens GN = NPM1 PE = 1 SV = 2	1.940886	0.0000862
48	sp|P55265|DSRAD_HUMAN	Double-stranded RNA-specific adenosine deaminase OS = Homo sapiens GN = ADAR PE = 1 SV = 4	1.923092	0.000118
49	sp|Q9UHB6|LIMA1_HUMAN	LIM domain and actin-binding protein 1 OS = Homo sapiens GN = LIMA1 PE = 1 SV = 1	1.923092	0.000813
50	sp|Q13423|NNTM_HUMAN	NAD(P) transhydrogenase, mitochondrial OS = Homo sapiens GN = NNT PE = 1 SV = 3	1.853532	0.0000358
51	sp|Q9Y2W1|TR150_HUMAN	Thyroid hormone receptor-associated protein 3 OS = Homo sapiens GN = THRAP3 PE = 1 SV = 2	1.836538	0.000124
52	sp|Q13263|TIF1B_HUMAN	Transcription intermediary factor 1-beta OS = Homo sapiens GN = TRIM28 PE = 1 SV = 5	1.786488	0.000475
53	sp|Q15149|PLEC_HUMAN	Plectin OS = Homo sapiens GN = PLEC PE = 1 SV = 3	1.584893	0.000000000695
54	sp|Q13813|SPTN1_HUMAN	Spectrin alpha chain, non-erythrocytic 1 OS = Homo sapiens GN = SPTAN1 PE = 1 SV = 3	1.555966	0.0000874
55	sp|Q9Y490|TLN1_HUMAN	Talin-1 OS = Homo sapiens GN = TLN1 PE = 1 SV = 3	0.60256	0.0000353

Table I. Cont.

No.	Accession	Name	FC	*P*-value
56	sp|Q14315|FLNC_HUMAN	Filamin-C OS = Homo sapiens GN = FLNC PE = 1 SV = 3	0.591562	0.00000147
57	sp|Q5T4S7|UBR4_HUMAN	E3 ubiquitin-protein ligase UBR4 OS = Homo sapiens GN = UBR4 PE = 1 SV = 1	0.559758	0.000653
58	sp|Q14152|EIF3A_HUMAN	Eukaryotic translation initiation factor 3 subunit A OS = Homo sapiens GN = EIF3A PE = 1 SV = 1	0.544503	0.000563
59	sp|Q14974|IMB1_HUMAN	Importin subunit beta-1 OS = Homo sapiens GN = KPNB1 PE = 1 SV = 2	0.515229	0.000226
60	sp|P41091|IF2G_HUMAN	Eukaryotic translation initiation factor 2 subunit 3 OS = Homo sapiens GN = EIF2S3 PE = 1 SV = 3	0.510505	0.000686
61	sp|P53621|COPA_HUMAN	Coatomer subunit alpha OS = Homo sapiens GN = COPA PE = 1 SV = 2	0.501187	0.000472
62	sp|Q16851|UGPA_HUMAN	UTP--glucose-1-phosphate uridylyltransferase OS = Homo sapiens GN = UGP2 PE = 1 SV = 5	0.501187	0.000532
63	sp|Q96P70|IPO9_HUMAN	Importin-9 OS = Homo sapiens GN = IPO9 PE = 1 SV = 3	0.501187	0.000168
64	sp|Q8WUM4|PDC6I_HUMAN	Programmed cell death 6-interacting protein OS = Homo sapiens GN = PDCD6IP PE = 1 SV = 1	0.49204	0.0000198
65	sp|P46940|IQGA1_HUMAN	Ras GTPase-activating-like protein IQGAP1 OS = Homo sapiens GN = IQGAP1 PE = 1 SV = 1	0.487529	0.000000907
66	sp|Q92973|TNPO1_HUMAN	Transportin-1 OS = Homo sapiens GN = TNPO1 PE = 1 SV = 2	0.483059	0.000241
67	sp|Q92598|HS105_HUMAN	Heat shock protein 105 kDa OS = Homo sapiens GN = HSPH1 PE = 1 SV = 1	0.47863	0.000511
68	sp|Q14204|DYHC1_HUMAN	Cytoplasmic dynein 1 heavy chain 1 OS = Homo sapiens GN = DYNC1H1 PE = 1 SV = 5	0.469894	0.000000000000591
69	sp|Q92616|GCN1_HUMAN	eIF-2-alpha kinase activator GCN1 OS = Homo sapiens GN = GCN1 PE = 1 SV = 6	0.465586	0.00000189
70	sp|P35579|MYH9_HUMAN	Myosin-9 OS = Homo sapiens GN = MYH9 PE = 1 SV = 4	0.461318	0.00000467
71	sp|P35606|COPB2_HUMAN	Coatomer subunit beta' OS = Homo sapiens GN = COPB2 PE = 1 SV = 2	0.461318	0.000382
72	sp|P27708|PYR1_HUMAN	CAD protein OS = Homo sapiens GN = CAD PE = 1 SV = 3	0.452898	0.00000122
73	sp|Q86VP6|CAND1_HUMAN	Cullin-associated NEDD8-dissociated protein 1 OS = Homo sapiens GN = CAND1 PE = 1 SV = 2	0.444631	0.00042
74	sp|P20073|ANXA7_HUMAN	Annexin A7 OS = Homo sapiens GN = ANXA7 PE = 1 SV = 3	0.42462	0.000415
75	sp|Q13228|SBP1_HUMAN	Selenium-binding protein 1 OS = Homo sapiens GN = SELENBP1 PE = 1 SV = 2	0.413047	0.00023
76	sp|Q96AC1|FERM2_HUMAN	Fermitin family homolog 2 OS = Homo sapiens GN = FERMT2 PE = 1 SV = 1	0.405508	0.0000768
77	sp|Q9UQ80|PA2G4_HUMAN	Proliferation-associated protein 2G4 OS = Homo sapiens GN = PA2G4 PE = 1 SV = 3	0.405508	0.000957
78	sp|P46821|MAP1B_HUMAN	Microtubule-associated protein 1B OS = Homo sapiens GN = MAP1B PE = 1 SV = 2	0.401791	0.0000993
79	sp|P40763|STAT3_HUMAN	Signal transducer and activator of transcription 3 OS = Homo sapiens GN = STAT3 PE = 1 SV = 2	0.390841	0.000108
80	sp|P22314|UBA1_HUMAN	Ubiquitin-like modifier-activating enzyme 1 OS = Homo sapiens GN = UBA1 PE = 1 SV = 3	0.387258	0.00000000036
81	sp|P34932|HSP74_HUMAN	Heat shock 70 kDa protein 4 OS = Homo sapiens GN = HSPA4 PE = 1 SV = 4	0.387258	0.000133
82	sp|P62826|RAN_HUMAN	GTP-binding nuclear protein Ran OS = Homo sapiens GN = RAN PE = 1 SV = 3	0.383707	0.000165
83	sp|P23526|SAHH_HUMAN	Adenosylhomocysteinase OS = Homo sapiens GN = AHCY PE = 1 SV = 4	0.383707	0.00032

Table I. Cont.

No.	Accession	Name	FC	*P*-value
84	sp|P27816|MAP4_HUMAN	Microtubule-associated protein 4 OS = Homo sapiens GN = MAP4 PE = 1 SV = 3	0.380189	0.0000000706
85	sp|P0DMV9|HS71B_HUMAN	Heat shock 70 kDa protein 1B OS = Homo sapiens GN = HSPA1B PE = 1 SV = 1	0.366438	0.00000206
86	sp|Q99832|TCPH_HUMAN	T-complex protein 1 subunit eta OS = Homo sapiens GN = CCT7 PE = 1 SV = 2	0.363078	0.000659
87	sp|Q99613|EIF3C_HUMAN	Eukaryotic translation initiation factor 3 subunit C OS = Homo sapiens GN = EIF3C PE = 1 SV = 1	0.356451	0.000267
88	sp|P48643|TCPE_HUMAN	T-complex protein 1 subunit epsilon OS = Homo sapiens GN = CCT5 PE = 1 SV = 1	0.353183	0.000000384
89	sp|P78344|IF4G2_HUMAN	Eukaryotic translation initiation factor 4 gamma 2 OS = Homo sapiens GN = EIF4G2 PE = 1 SV = 1	0.353183	0.000055
90	sp|P23921|RIR1_HUMAN	Ribonucleoside-diphosphate reductase large subunit OS = Homo sapiens GN = RRM1 PE = 1 SV = 1	0.343558	0.0000000196
91	sp|Q06210|GFPT1_HUMAN	Glutamine--fructose-6-phosphate aminotransferase [isomerizing] 1 OS = Homo sapiens GN = GFPT1 PE = 1 SV = 3	0.337287	0.000328
92	sp|Q9BXJ9|NAA15_HUMAN	N-alpha-acetyltransferase 15, NatA auxiliary subunit OS = Homo sapiens GN = NAA15 PE = 1 SV = 1	0.331131	0.0000275
93	sp|P49368|TCPG_HUMAN	T-complex protein 1 subunit gamma OS = Homo sapiens GN = CCT3 PE = 1 SV = 4	0.328095	0.0000143
94	sp|O75083|WDR1_HUMAN	WD repeat-containing protein 1 OS = Homo sapiens GN = WDR1 PE = 1 SV = 4	0.322107	0.00061
95	sp|P55786|PSA_HUMAN	Puromycin-sensitive aminopeptidase OS = Homo sapiens GN = NPEPPS PE = 1 SV = 2	0.316228	0.000026
96	sp|P09960|LKHA4_HUMAN	Leukotriene A-4 hydrolase OS = Homo sapiens GN = LTA4H PE = 1 SV = 2	0.316228	0.0000935
97	sp|P30520|PURA2_HUMAN	Adenylosuccinate synthetase isozyme 2 OS = Homo sapiens GN = ADSS PE = 1 SV = 3	0.316228	0.0000165
98	sp|Q15691|MARE1_HUMAN	Microtubule-associated protein RP/EB family member 1 OS = Homo sapiens GN = MAPRE1 PE = 1 SV = 3	0.316228	0.000408
99	sp|P12814|ACTN1_HUMAN	Alpha-actinin-1 OS = Homo sapiens GN = ACTN1 PE = 1 SV = 2	0.313329	0.000176
100	sp|P30044|PRDX5_HUMAN	Peroxiredoxin-5, mitochondrial OS = Homo sapiens GN = PRDX5 PE = 1 SV = 4	0.313329	0.000749
101	sp|P78371|TCPB_HUMAN	T-complex protein 1 subunit beta OS = Homo sapiens GN = CCT2 PE = 1 SV = 4	0.30479	0.000000242
102	sp|P54136|SYRC_HUMAN	Arginine--tRNA ligase, cytoplasmic OS = Homo sapiens GN = RARS PE = 1 SV = 2	0.30479	0.000287
103	sp|P50991|TCPD_HUMAN	T-complex protein 1 subunit delta OS = Homo sapiens GN = CCT4 PE = 1 SV = 4	0.30479	0.0000303
104	sp|P23588|IF4B_HUMAN	Eukaryotic translation initiation factor 4B OS = Homo sapiens GN = EIF4B PE = 1 SV = 2	0.30479	0.00000105
105	sp|P13489|RINI_HUMAN	Ribonuclease inhibitor OS = Homo sapiens GN = RNH1 PE = 1 SV = 2	0.30479	0.000529
106	sp|P55263|ADK_HUMAN	Adenosine kinase OS = Homo sapiens GN = ADK PE = 1 SV = 2	0.301995	0.000591
107	sp|P40227|TCPZ_HUMAN	T-complex protein 1 subunit zeta OS = Homo sapiens GN = CCT6A PE = 1 SV = 3	0.296483	0.000029
108	sp|P15559|NQO1_HUMAN	NAD(P)H dehydrogenase [quinone] 1 OS = Homo sapiens GN = NQO1 PE = 1 SV = 1	0.296483	0.000441
109	sp|P50990|TCPQ_HUMAN	T-complex protein 1 subunit theta OS = Homo sapiens GN = CCT8 PE = 1 SV = 4	0.291072	0.000000345
110	sp|P31947|1433S_HUMAN	14-3-3 protein sigma OS = Homo sapiens GN = SFN PE = 1 SV = 1	0.285759	0.000365

Table I. Cont.

No.	Accession	Name	FC	*P*-value
111	sp|Q16658|FSCN1_HUMAN	Fascin OS = Homo sapiens GN = FSCN1 PE = 1 SV = 3	0.280543	0.00000154
112	sp|Q01518|CAP1_HUMAN	Adenylyl cyclase-associated protein 1 OS = Homo sapiens GN = CAP1 PE = 1 SV = 5	0.275423	0.0000322
113	sp|P00966|ASSY_HUMAN	Argininosuccinate synthase OS = Homo sapiens GN = ASS1 PE = 1 SV = 2	0.272898	0.0000194
114	sp|P60981|DEST_HUMAN	Destrin OS = Homo sapiens GN = DSTN PE = 1 SV = 3	0.272898	0.0000395
115	sp|P52209|6PGD_HUMAN	6-phosphogluconate dehydrogenase, decarboxylating OS = Homo sapiens GN = PGD PE = 1 SV = 3	0.270396	0.0000138
116	sp|Q9Y2T3|GUAD_HUMAN	Guanine deaminase OS = Homo sapiens GN = GDA PE = 1 SV = 1	0.270396	0.000249
117	sp|Q7L1Q6|BZW1_HUMAN	Basic leucine zipper and W2 domain-containing protein 1 OS = Homo sapiens GN = BZW1 PE = 1 SV = 1	0.265461	0.000453
118	sp|Q16401|PSMD5_HUMAN	26S proteasome non-ATPase regulatory subunit 5 OS = Homo sapiens GN = PSMD5 PE = 1 SV = 3	0.260615	0.00000517
119	sp|P16152|CBR1_HUMAN	Carbonyl reductase [NADPH] 1 OS = Homo sapiens GN = CBR1 PE = 1 SV = 3	0.260615	0.00017
120	sp|Q9NTK5|OLA1_HUMAN	Obg-like ATPase 1 OS = Homo sapiens GN = OLA1 PE = 1 SV = 2	0.258226	0.000491
121	sp|P11586|C1TC_HUMAN	C-1-tetrahydrofolate synthase, cytoplasmic OS = Homo sapiens GN = MTHFD1 PE = 1 SV = 3	0.253513	0.00000226
122	sp|P40925|MDHC_HUMAN	Malate dehydrogenase, cytoplasmic OS = Homo sapiens GN = MDH1 PE = 1 SV = 4	0.251189	0.00000186
123	sp|O95373|IPO7_HUMAN	Importin-7 OS = Homo sapiens GN = IPO7 PE = 1 SV = 1	0.244343	0.000934
124	sp|Q9Y617|SERC_HUMAN	Phosphoserine aminotransferase OS = Homo sapiens GN = PSAT1 PE = 1 SV = 2	0.244343	0.0000026
125	sp|P54578|UBP14_HUMAN	Ubiquitin carboxyl-terminal hydrolase 14 OS = Homo sapiens GN = USP14 PE = 1 SV = 3	0.235505	0.000113
126	sp|P36952|SPB5_HUMAN	Serpin B5 OS = Homo sapiens GN = SERPINB5 PE = 1 SV = 2	0.235505	0.0000299
127	sp|Q9UGI8|TES_HUMAN	Testin OS = Homo sapiens GN = TES PE = 1 SV = 1	0.235505	0.000587
128	sp|P49588|SYAC_HUMAN	Alanine--tRNA ligase, cytoplasmic OS = Homo sapiens GN = AARS PE = 1 SV = 2	0.233346	0.000000015
129	sp|P54577|SYYC_HUMAN	Tyrosine--tRNA ligase, cytoplasmic OS = Homo sapiens GN = YARS PE = 1 SV = 4	0.231207	0.000000451
130	sp|Q16719|KYNU_HUMAN	Kynureninase OS = Homo sapiens GN = KYNU PE = 1 SV = 1	0.229087	0.000151
131	sp|P07900|HS90A_HUMAN	Heat shock protein HSP 90-alpha OS = Homo sapiens GN = HSP90AA1 PE = 1 SV = 5	0.226986	0.00000039
132	sp|P23381|SYWC_HUMAN	Tryptophan--tRNA ligase, cytoplasmic OS = Homo sapiens GN = WARS PE = 1 SV = 2	0.224906	0.0000214
133	sp|P50395|GDIB_HUMAN	Rab GDP dissociation inhibitor beta OS = Homo sapiens GN = GDI2 PE = 1 SV = 2	0.218776	0.000381
134	sp|P21266|GSTM3_HUMAN	Glutathione S-transferase Mu 3 OS = Homo sapiens GN = GSTM3 PE = 1 SV = 3	0.218776	0.0000181
135	sp|Q01813|PFKAP_HUMAN	ATP-dependent 6-phosphofructokinase, platelet type OS = Homo sapiens GN = PFKP PE = 1 SV = 2	0.21677	0.0000109
136	sp|P29401|TKT_HUMAN	Transketolase OS = Homo sapiens GN = TKT PE = 1 SV = 3	0.214783	0.00000818
137	sp|O14980|XPO1_HUMAN	Exportin-1 OS = Homo sapiens GN = XPO1 PE = 1 SV = 1	0.214783	0.0000144
138	sp|P35237|SPB6_HUMAN	Serpin B6 OS = Homo sapiens GN = SERPINB6 PE = 1 SV = 3	0.214783	0.000441

Table I. Cont.

No.	Accession	Name	FC	*P*-value
139	sp|P26038|MOES_HUMAN	Moesin OS = Homo sapiens GN = MSN PE = 1 SV = 3	0.212814	0.000000083
140	sp|P60174|TPIS_HUMAN	Triosephosphate isomerase OS = Homo sapiens GN = TPI1 PE = 1 SV = 3	0.210863	0.000000565
141	sp|P17987|TCPA_HUMAN	T-complex protein 1 subunit alpha OS = Homo sapiens GN = TCP1 PE = 1 SV = 1	0.210863	0.00000355
142	sp|P37837|TALDO_HUMAN	Transaldolase OS = Homo sapiens GN = TALDO1 PE = 1 SV = 2	0.210863	0.00002
143	sp|P00491|PNPH_HUMAN	Purine nucleoside phosphorylase OS = Homo sapiens GN = PNP PE = 1 SV = 2	0.210863	0.000182
144	sp|P12429|ANXA3_HUMAN	Annexin A3 OS = Homo sapiens GN = ANXA3 PE = 1 SV = 3	0.207014	0.000102
145	sp|P60842|IF4A1_HUMAN	Eukaryotic initiation factor 4A-I OS = Homo sapiens GN = EIF4A1 PE = 1 SV = 1	0.205116	0.00039
146	sp|P08133|ANXA6_HUMAN	Annexin A6 OS = Homo sapiens GN = ANXA6 PE = 1 SV = 3	0.203236	0.0000209
147	sp|P22102|PUR2_HUMAN	Trifunctional purine biosynthetic protein adenosine-3 OS = Homo sapiens GN = GART PE = 1 SV = 1	0.201372	0.00000215
148	sp|Q16881|TRXR1_HUMAN	Thioredoxin reductase 1, cytoplasmic OS = Homo sapiens GN = TXNRD1 PE = 1 SV = 3	0.199526	0.00000000739
149	sp|P35241|RADI_HUMAN	Radixin OS = Homo sapiens GN = RDX PE = 1 SV = 1	0.199526	0.0000185
150	sp|P30085|KCY_HUMAN	UMP-CMP kinase OS = Homo sapiens GN = CMPK1 PE = 1 SV = 3	0.192309	0.000245
151	sp|P17812|PYRG1_HUMAN	CTP synthase 1 OS = Homo sapiens GN = CTPS1 PE = 1 SV = 2	0.188799	0.000024
152	sp|P49327|FAS_HUMAN	Fatty acid synthase OS = Homo sapiens GN = FASN PE = 1 SV = 3	0.183654	0,00
153	sp|P08238|HS90B_HUMAN	Heat shock protein HSP 90-beta OS = Homo sapiens GN = HSP90AB1 PE = 1 SV = 4	0.183654	0.0000176
154	sp|P31939|PUR9_HUMAN	Bifunctional purine biosynthesis protein PURH OS = Homo sapiens GN = ATIC PE = 1 SV = 3	0.183654	0.000000181
155	sp|P36871|PGM1_HUMAN	Phosphoglucomutase-1 OS = Homo sapiens GN = PGM1 PE = 1 SV = 3	0.183654	0.00000167
156	sp|P18669|PGAM1_HUMAN	Phosphoglycerate mutase 1 OS = Homo sapiens GN = PGAM1 PE = 1 SV = 2	0.183654	0.000112
157	sp|P11413|G6PD_HUMAN	Glucose-6-phosphate 1-dehydrogenase OS = Homo sapiens GN = G6PD PE = 1 SV = 4	0.177011	0.00000103
158	sp|P17655|CAN2_HUMAN	Calpain-2 catalytic subunit OS = Homo sapiens GN = CAPN2 PE = 1 SV = 6	0.177011	0.00000121
159	sp|O43175|SERA_HUMAN	D-3-phosphoglycerate dehydrogenase OS = Homo sapiens GN = PHGDH PE = 1 SV = 4	0.175388	0.0000184
160	sp|P04075|ALDOA_HUMAN	Fructose-bisphosphate aldolase A OS = Homo sapiens GN = ALDOA PE = 1 SV = 2	0.17378	0.0000134
161	sp|P41250|SYG_HUMAN	Glycine--tRNA ligase OS = Homo sapiens GN = GARS PE = 1 SV = 3	0.17378	0.000000134
162	sp|O75874|IDHC_HUMAN	Isocitrate dehydrogenase [NADP] cytoplasmic OS = Homo sapiens GN = IDH1 PE = 1 SV = 2	0.172187	0.000000103
163	sp|P18206|VINC_HUMAN	Vinculin OS = Homo sapiens GN = VCL PE = 1 SV = 4	0.170608	0,00
164	sp|P31948|STIP1_HUMAN	Stress-induced-phosphoprotein 1 OS = Homo sapiens GN = STIP1 PE = 1 SV = 1	0.158489	0.0000000108
165	sp|P53396|ACLY_HUMAN	ATP-citrate synthase OS = Homo sapiens GN = ACLY PE = 1 SV = 3	0.157036	0.000000000426
166	sp|Q9Y266|NUDC_HUMAN	Nuclear migration protein nudC OS = Homo sapiens GN = NUDC PE = 1 SV = 1	0.157036	0.000000195

Table I. Cont.

No.	Accession	Name	FC	*P*-value
167	sp|P55060|XPO2_HUMAN	Exportin-2 OS = Homo sapiens GN = CSE1L PE = 1 SV = 3	0.155597	0.00000000656
168	sp|O43776|SYNC_HUMAN	Asparagine--tRNA ligase, cytoplasmic OS = Homo sapiens GN = NARS PE = 1 SV = 1	0.155597	0.0000275
169	sp|P13797|PLST_HUMAN	Plastin-3 OS = Homo sapiens GN = PLS3 PE = 1 SV = 4	0.148594	0.000000327
170	sp|Q14914|PTGR1_HUMAN	Prostaglandin reductase 1 OS = Homo sapiens GN = PTGR1 PE = 1 SV = 2	0.143219	0.000000538
171	sp|P62258|1433E_HUMAN	14-3-3 protein epsilon OS = Homo sapiens GN = YWHAE PE = 1 SV = 1	0.138038	0.0000521
172	sp|P26639|SYTC_HUMAN	Threonine--tRNA ligase, cytoplasmic OS = Homo sapiens GN = TARS PE = 1 SV = 3	0.136773	0.000000000522
173	sp|P27348|1433T_HUMAN	14-3-3 protein theta OS = Homo sapiens GN = YWHAQ PE = 1 SV = 1	0.131826	0.0000612
174	sp|Q15185|TEBP_HUMAN	Prostaglandin E synthase 3 OS = Homo sapiens GN = PTGES3 PE = 1 SV = 1	0.12942	0.000842
175	sp|P00338|LDHA_HUMAN	L-lactate dehydrogenase A chain OS = Homo sapiens GN = LDHA PE = 1 SV = 2	0.128233	0.00000000672
176	sp|P08758|ANXA5_HUMAN	Annexin A5 OS = Homo sapiens GN = ANXA5 PE = 1 SV = 2	0.128233	0.000000000417
177	sp|Q15181|IPYR_HUMAN	Inorganic pyrophosphatase OS = Homo sapiens GN = PPA1 PE = 1 SV = 2	0.128233	0.0000608
178	sp|P07195|LDHB_HUMAN	L-lactate dehydrogenase B chain OS = Homo sapiens GN = LDHB PE = 1 SV = 2	0.122462	0.0000861
179	sp|P06733|ENOA_HUMAN	Alpha-enolase OS = Homo sapiens GN = ENO1 PE = 1 SV = 2	0.115878	0.0000000119
180	sp|Q06830|PRDX1_HUMAN	Peroxiredoxin-1 OS = Homo sapiens GN = PRDX1 PE = 1 SV = 1	0.104713	0.000282
181	sp|P13639|EF2_HUMAN	Elongation factor 2 OS = Homo sapiens GN = EEF2 PE = 1 SV = 4	0.102802	0.0000215
182	sp|O00299|CLIC1_HUMAN	Chloride intracellular channel protein 1 OS = Homo sapiens GN = CLIC1 PE = 1 SV = 4	0.102802	0.000245
183	sp|P15311|EZRI_HUMAN	Ezrin OS = Homo sapiens GN = EZR PE = 1 SV = 4	0.1	0.0000000224
184	sp|P15121|ALDR_HUMAN	Aldose reductase OS = Homo sapiens GN = AKR1B1 PE = 1 SV = 3	0.099083	0.00000144
185	sp|P37802|TAGL2_HUMAN	Transgelin-2 OS = Homo sapiens GN = TAGLN2 PE = 1 SV = 3	0.095499	0.0000496
186	sp|P06744|G6PI_HUMAN	Glucose-6-phosphate isomerase OS = Homo sapiens GN = GPI PE = 1 SV = 4	0.091201	0.0000000011
187	sp|P00558|PGK1_HUMAN	Phosphoglycerate kinase 1 OS = Homo sapiens GN = PGK1 PE = 1 SV = 3	0.083946	0.00000202
188	sp|P30041|PRDX6_HUMAN	Peroxiredoxin-6 OS = Homo sapiens GN = PRDX6 PE = 1 SV = 3	0.079433	0.000000231
189	sp|Q01581|HMCS1_HUMAN	Hydroxymethylglutaryl-CoA synthase, cytoplasmic OS = Homo sapiens GN = HMGCS1 PE = 1 SV = 2	0.06792	0.0000000145
190	sp|P12725|A1AT_SHEEP	Alpha-1-antiproteinase OS = Ovis aries PE = 1 SV = 1	0.064269	0.0000536

Table II. Differentially expressed proteins identified between adjacent noncancerous tissues and distal noncancerous tissues of hepatocellular carcinoma

No.	Accession	Name	FC	*P*-value
1	sp|P12763|FETUA_BOVIN	Alpha-2-HS-glycoprotein OS = Bos taurus GN = AHSG PE = 1 SV = 2	4.37	0.000000647
2	sp|O00299|CLIC1_HUMAN	Chloride intracellular channel protein 1 OS = Homo sapiens GN = CLIC1 PE = 1 SV = 4	3.49945211	0.00064666
3	sp|P78417|GSTO1_HUMAN	Glutathione S-transferase omega-1 OS = Homo sapiens GN = GSTO1 PE = 1 SV = 2	3.46736908	0.00088023
4	sp|P00558|PGK1_HUMAN	Phosphoglycerate kinase 1 OS = Homo sapiens GN = PGK1 PE = 1 SV = 3	3.34	0.000000494
5	sp|P17812|PYRG1_HUMAN	CTP synthase 1 OS = Homo sapiens GN = CTPS1 PE = 1 SV = 2	3.28095293	0.00090827
6	sp|Q01813|PFKAP_HUMAN	ATP-dependent 6-phosphofructokinase. platelet type OS = Homo sapiens GN = PFKP PE = 1 SV = 2	3.2210691	0.00021282
7	sp|P06744|G6PI_HUMAN	Glucose-6-phosphate isomerase OS = Homo sapiens GN = GPI PE = 1 SV = 4	3.16	0.00000522
8	sp|P04264|K2C1_HUMAN	Keratin. type II cytoskeletal 1 OS = Homo sapiens GN = KRT1 PE = 1 SV = 6	3.133286	0.00012301
9	sp|P21266|GSTM3_HUMAN	Glutathione S-transferase Mu 3 OS = Homo sapiens GN = GSTM3 PE = 1 SV = 3	2.88	0.0000379
10	sp|P30041|PRDX6_HUMAN	Peroxiredoxin-6 OS = Homo sapiens GN = PRDX6 PE = 1 SV = 3	2.83139205	0.00092527
11	sp|P08133|ANXA6_HUMAN	Annexin A6 OS = Homo sapiens GN = ANXA6 PE = 1 SV = 3	2.83139205	0.00077018
12	sp|P31939|PUR9_HUMAN	Bifunctional purine biosynthesis protein PURH OS = Homo sapiens GN = ATIC PE = 1 SV = 3	2.56	0.0000395
13	sp|P36871|PGM1_HUMAN	Phosphoglucomutase-1 OS = Homo sapiens GN = PGM1 PE = 1 SV = 3	2.49	0.00000426
14	sp|Q15181|IPYR_HUMAN	Inorganic pyrophosphatase OS = Homo sapiens GN = PPA1 PE = 1 SV = 2	2.48885703	0.00020884
15	sp|Q96P70|IPO9_HUMAN	Importin-9 OS = Homo sapiens GN = IPO9 PE = 1 SV = 3	2.46603894	0.00095205
16	sp|P50395|GDIB_HUMAN	Rab GDP dissociation inhibitor beta OS = Homo sapiens GN = GDI2 PE = 1 SV = 2	2.38	0.0000832
17	sp|P00491|PNPH_HUMAN	Purine nucleoside phosphorylase OS = Homo sapiens GN = PNP PE = 1 SV = 2	2.37684011	0.00012449
18	sp|Q9Y617|SERC_HUMAN	Phosphoserine aminotransferase OS = Homo sapiens GN = PSAT1 PE = 1 SV = 2	2.26986504	0.00016311
19	sp|P55060|XPO2_HUMAN	Exportin-2 OS = Homo sapiens GN = CSE1L PE = 1 SV = 3	2.25	0.00000809
20	sp|P13797|PLST_HUMAN	Plastin-3 OS = Homo sapiens GN = PLS3 PE = 1 SV = 4	2.051162	0.00014754
21	sp|Q01581|HMCS1_HUMAN	Hydroxymethylglutaryl-CoA synthase. cytoplasmic OS = Homo sapiens GN = HMGCS1 PE = 1 SV = 2	1.95884502	0.00053098
22	sp|P18206|VINC_HUMAN	Vinculin OS = Homo sapiens GN = VCL PE = 1 SV = 4	1.91	0.00000266

Table II. Cont.

No.	Accession	Name	FC	*P*-value
23	sp|P49588|SYAC_HUMAN	Alanine-tRNA ligase. cytoplasmic OS = Homo sapiens GN = AARS PE = 1 SV = 2	1.87	0.0000459
24	sp|P49327|FAS_HUMAN	Fatty acid synthase OS = Homo sapiens GN = FASN PE = 1 SV = 3	1.85	0.000000763
25	sp|P11413|G6PD_HUMAN	Glucose-6-phosphate 1-dehydrogenase OS = Homo sapiens GN = G6PD PE = 1 SV = 4	1.80301797	0.00072658
26	sp|Q86UP2|KTN1_HUMAN	Kinectin OS = Homo sapiens GN = KTN1 PE = 1 SV = 1	0.60255963	0.00045493
27	sp|P13667|PDIA4_HUMAN	Protein disulfide-isomerase A4 OS = Homo sapiens GN = PDIA4 PE = 1 SV = 2	0.603	0.0000523
28	sp|P25705|ATPA_HUMAN	ATP synthase subunit alpha. mitochondrial OS = Homo sapiens GN = ATP5A1 PE = 1 SV = 1	0.53951061	0.00031264
29	sp|O75369|FLNB_HUMAN	Filamin-B OS = Homo sapiens GN = FLNB PE = 1 SV = 2	0.535	0.000067
30	sp|P31327|CPSM_HUMAN	Carbamoyl-phosphate synthase [ammonia]. mitochondrial OS = Homo sapiens GN = CPS1 PE = 1 SV = 2	0.492	0.00000077
31	sp|Q9P2E9|RRBP1_HUMAN	Ribosome-binding protein 1 OS = Homo sapiens GN = RRBP1 PE = 1 SV = 4	0.488	0.0000851
32	sp|Q14126|DSG2_HUMAN	Desmoglein-2 OS = Homo sapiens GN = DSG2 PE = 1 SV = 2	0.40550849	0.00097142
33	sp|P30050|RL12_HUMAN	60S ribosomal protein L12 OS = Homo sapiens GN = RPL12 PE = 1 SV = 1	0.38725761	0.00062865
34	sp|P40926|MDHM_HUMAN	Malate dehydrogenase. mitochondrial OS = Homo sapiens GN = MDH2 PE = 1 SV = 3	0.37325019	0.00081137
35	sp|Q07065|CKAP4_HUMAN	Cytoskeleton-associated protein 4 OS = Homo sapiens GN = CKAP4 PE = 1 SV = 2	0.366	0.00000472
36	sp|P23246|SFPQ_HUMAN	Splicing factor. proline- and glutamine-rich OS = Homo sapiens GN = SFPQ PE = 1 SV = 2	0.36307809	0.00011904
37	sp|Q8IVF2|AHNK2_HUMAN	Protein AHNAK2 OS = Homo sapiens GN = AHNAK2 PE = 1 SV = 2	0.36	0.0000000183
38	sp|Q13813|SPTN1_HUMAN	Spectrin alpha chain. non-erythrocytic 1 OS = Homo sapiens GN = SPTAN1 PE = 1 SV = 3	0.344	0.0000000289
39	sp|P19338|NUCL_HUMAN	Nucleolin OS = Homo sapiens GN = NCL PE = 1 SV = 3	0.316	0.000000799
40	sp|P11021|GRP78_HUMAN	78 kDa glucose-regulated protein OS = Homo sapiens GN = HSPA5 PE = 1 SV = 2	0.27	0.000000000617
41	sp|P27824|CALX_HUMAN	Calnexin OS = Homo sapiens GN = CANX PE = 1 SV = 2	0.2558586	0.0005111
42	sp|P46779|RL28_HUMAN	60S ribosomal protein L28 OS = Homo sapiens GN = RPL28 PE = 1 SV = 3	0.237684	0.00034004
43	sp|P10809|CH60_HUMAN	60 kDa heat shock protein. mitochondrial OS = Homo sapiens GN = HSPD1 PE = 1 SV = 2	0.215	0.000000000379
44	sp|P08670|VIME_HUMAN	Vimentin OS = Homo sapiens GN = VIM PE = 1 SV = 4	0.175	0.00000297

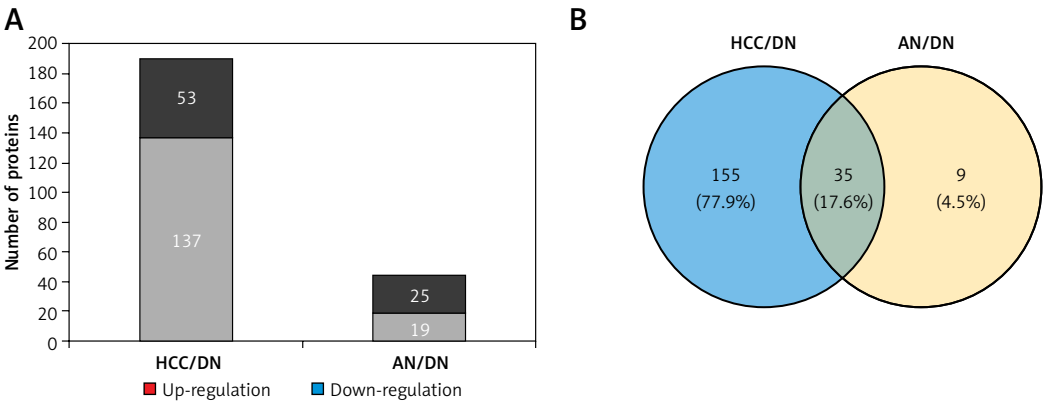

Figure 2. Features of the hepatocellular carcinoma secretome dataset from the isobaric tags for relative and absolute quantification shotgun analysis. **A** – The distribution of differently abundant proteins in 2 groups. **B** – Venn diagrams show the numbers of the identified proteins and the overlaps of differently abundant proteins in the 2 groups

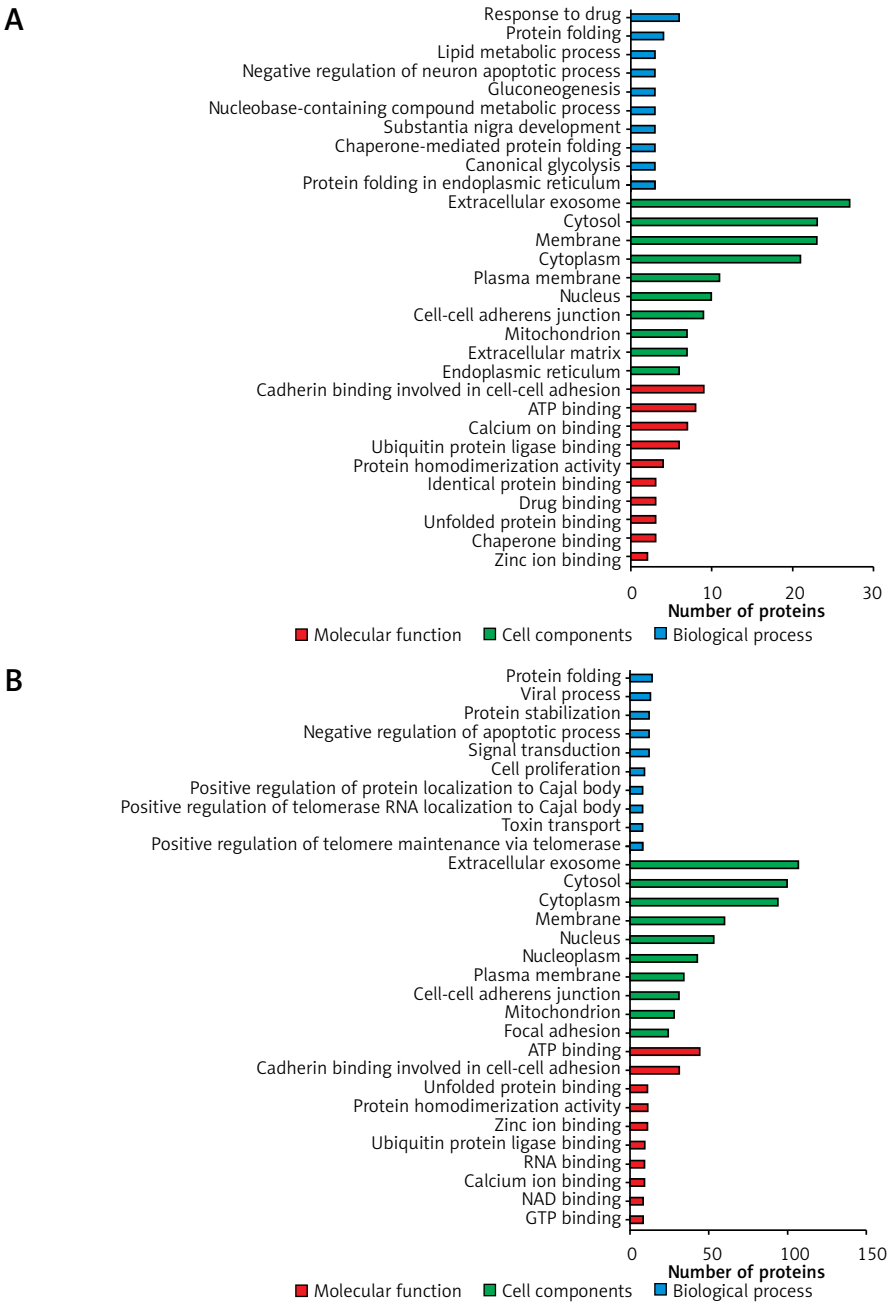

Figure 3. The gene ontology (GO) analysis of the differently abundant proteins. **A** – The GO analysis of differently abundant proteins overlapped in the 2 groups. **B** – The GO analysis of differently abundant proteins only involved in the hepatocellular carcinoma tissues/distal noncancerous tissues group

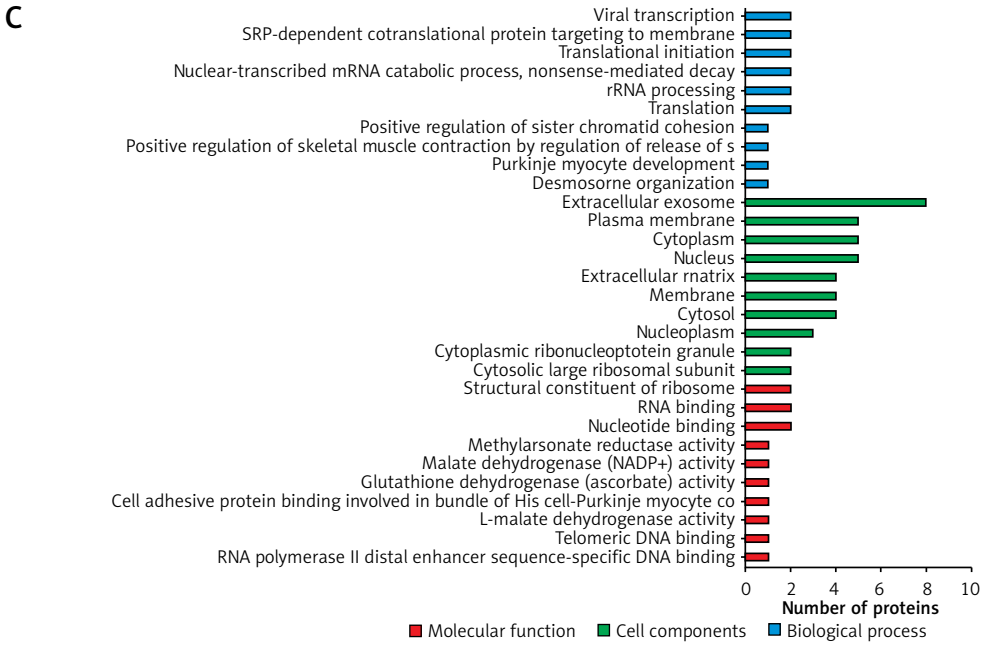

Figure 3. Cont. **C** – The GO analysis of differently abundant proteins only involved in the adjacent noncancerous tissues/distal noncancerous tissues group

acids metabolism, trichloroacetic acid (TCA) cycle, glucose metabolism, etc.

The String analysis of the differentially expressed proteins

As shown in Figure 5 A, in the HCC/DN group, the proteins could be classified into 3 major clusters: proteins in the red region were related to protein translation and post-translation processing, proteins in the blue region were related to protein glycosylation modification, and proteins in the green region were related to biological metabolic functions dominated by glucose metabolism. While in the AN/DN group, the proteins could also be classified into 3 clusters: the red region represented proteins related to immune and metabolic functions, the green region represented proteins related to apoptosis functions, and the blue region represented proteins related to protein binding functions (Figure 5 B).

Discussion

Hepatocellular carcinoma has become the third-most-common cause of cancer-related death worldwide. Most cases of HCC were developed in patients who had already had liver cirrhosis [15]. Therefore, surveillance for the early onset of HCC was recommended. The biomarkers with high sensitivity and specificity were essential for optimising the management of HCC [16]. Zhang *et al*. used the iTRAQ pipeline to distinguish the proteomic profiles of malignant ascites in HCC patients from those with non-malignant liver cirrhosis and found that Enolase-1 and fibrinogen are potential ascitic fluid-based biomarkers for diagnosis and prognosis of HCC [17]. Guo *et al*. reported that assaying CD14 levels may complement AFP measurement for the early detection of HCC [18]. Wang *et al*. suggested that different molecular alterations and specific signalling pathways were indeed involved in different HCC subtypes [19]. Our study aimed to investigate the molecular signatures of the HCC by quantitative proteomics using iTRAQ with LC-MS/MS.

In our study, the number of differentially expressed proteins identified in the HCC/DN group was much higher than in the AN/DN group. These findings indicate that the features between the adjacent noncancerous tissues and distant noncancerous tissues were more similar than those between the HCC tissues and the distant noncancerous tissues, which were accorded with objective existence.

The gene ontology annotation analysis showed that the cell components of the differentially expressed proteins that either overlapped in 2 groups or uniquely in 1 group were mostly located in the extracellular exosome, which indicated that the proteins extracted in this experiment were mainly secreted proteins. For the biological process analysis, the GO annotation analysis showed that the proteins overlapped in both the groups and were the major participants in the protein folding, lipid metabolic process, gluconeogenesis, nucleobase-containing compound metabolic process, and canonical glycolysis. Most of these processes focused on metabolic changes, which

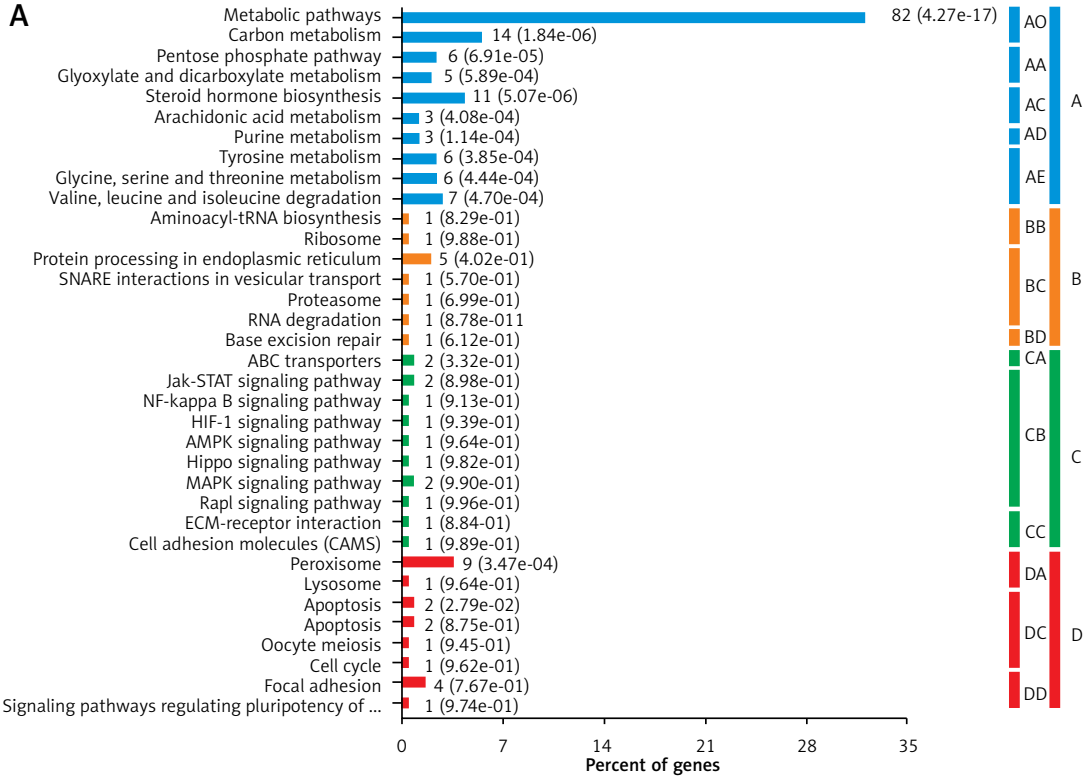

A : Metabolism
AO : Global and overview maps
AA : Carbohydrate metabolism
AC : Lipid metabolism
AD : Nucleotide metabolism
AE : Amino acid metabolism

B : Genetic Information Processing
BB : Translation
BC : Folding, sorting and degradation
BD : Replication and repair

C : Environmental Information Processing
CA : Membrane transport
CB : Signal transduction
CC : Signaling molecules and interaction

D : Cellular Processes
DA : Transport and catabolism
DC : Cell growth and death
DO : Cellular community

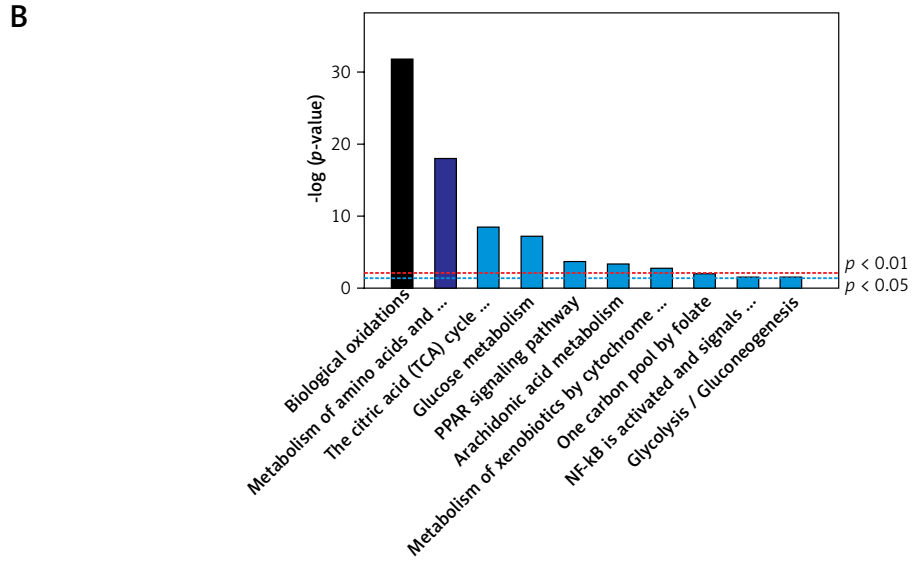

Figure 4. The key signalling pathways involved in the 2 groups. **A** – The key signalling pathways involved in the hepatocellular carcinoma tissues/distal noncancerous tissues group. **B** – The key signalling pathways involved in the adjacent noncancerous tissues/distal noncancerous tissues group. The top 10 enriched signalling pathways were displayed in the figures

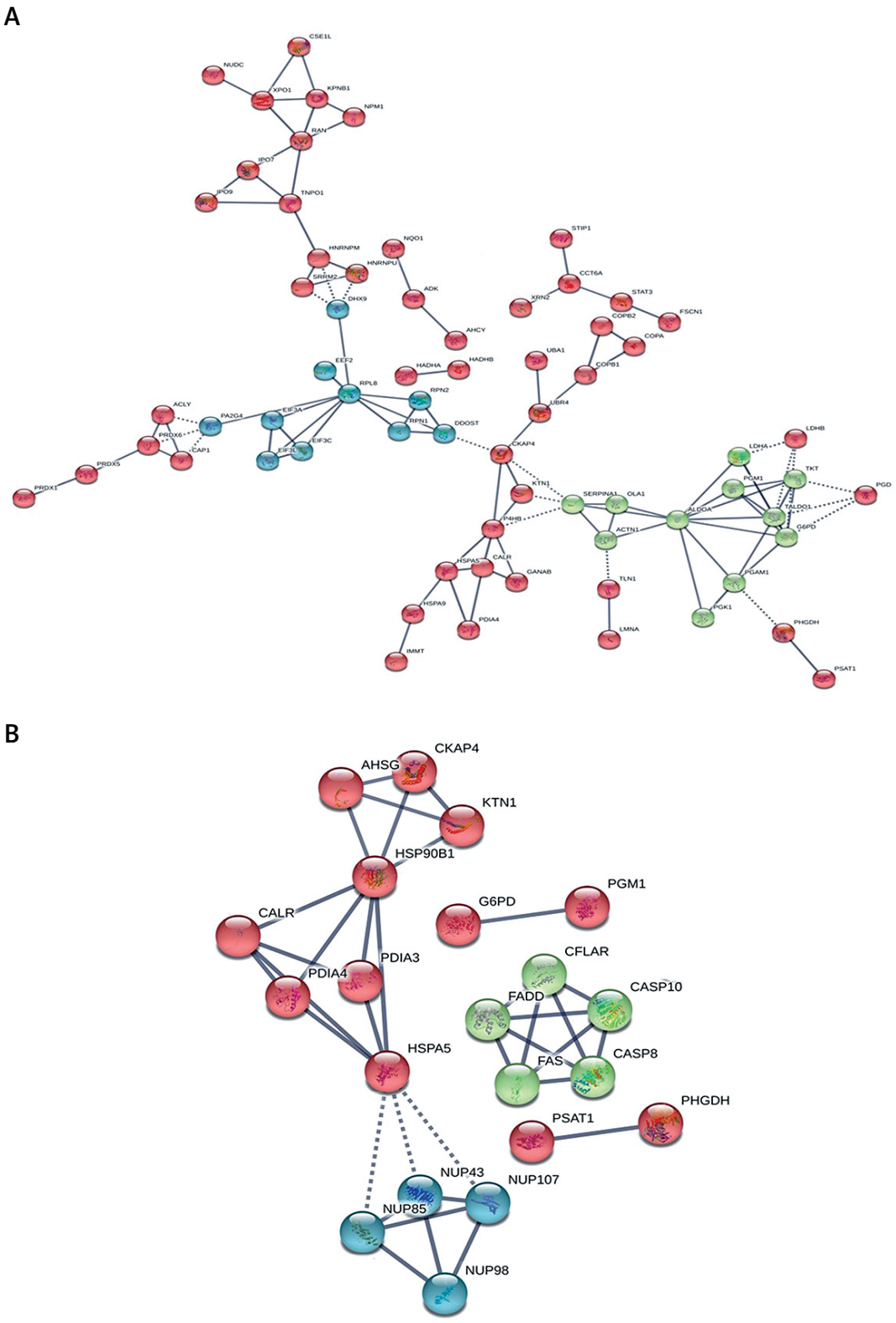

Figure 5. The interaction networks of differently abundant proteins in the 2 groups. **A** – The interaction networks of differently abundant proteins involved in the hepatocellular carcinoma tissues/distal noncancerous tissues group. **B** – The interaction networks of differently abundant proteins involved in the adjacent noncancerous tissues/distal noncancerous tissues group

suggested that the changes in the material metabolism were universal, regardless of the transformation from distant cancer to adjacent cancer or the approach of adjacent cancer to HCC. The molecular function of these proteins also focuses on energy metabolism, which also supported the hypothesis [15, 20–23].

There were 155 dysregulated proteins in the HCC group compared to the DN group, but these proteins were not dysregulated in the AN group compared to the DN group. We further analysed that these proteins involved the biological process by GO analysis; the results showed that these dysregulated proteins were mainly involved in signal transduction, cell proliferation, protein stabilisation, and the negative regulation of the apoptotic process. These processes might be involved in the formation or development of HCC, and it has been reported that these processes are involved in the disturbing of the signal transduction and protein degradation [24–27], apoptotic process [27, 28], and cell proliferation [28, 29] in tumours. The molecular function of these proteins, such as the cadherin binding involved in cell-cell adhesion, protein homodimerisation activity, ubiquitin-protein ligase binding, calcium ion binding, GTP binding, etc., also supported this conclusion.

Interestingly, there were 9 dysregulated proteins in the AN group compared to the DN group but no dysregulation in the HCC group compared to the DN group, and the GO results showed that these dysregulated proteins were mainly involved in desmosome organisation, positive regulation of sister chromatid cohesion, translation, rRNA processing, nuclear-transcribed mRNA catabolic process, translational initiation, and SRP-dependent co-translational protein targeting the membrane. The results also showed that the dysregulated proteins may have affected the incidence and progress of HCC, such as the change of the combination of the protein and the RNA function presenting the disorder of the transcription and translation function, which suggested that the surrounding noncancerous cells might increase the expression of the nucleic acid and enzyme by tumour microenvironment to promote the HCC proliferation and growth [30], and that the changes of telomere and telomerase in the surrounding noncancerous cells revealed the dysregulation on the chromosome stability, repair, and proliferation, which were all closely related to the incidence of HCC development [31, 32]. Similarly, the molecular function of these proteins, such as cadherin binding-involved nucleotide binding, RNA binding, calcium ion binding, chromatin binding, transcription regulatory region DNA binding, identical protein binding, etc., also supported this conclusion.

To further reveal the possible molecular mechanisms of the tumourigenesis and the development of the primary HCC, we applied the KEGG database to analyse the signalling pathways in which the differentially expressed proteins were involved. Our study also analysed the pathway of metabolism, genetic information processing, environmental information processing, and cellular. According to the results of the analysis, the dysregulated proteins in HCC are mostly involved in the JAK-STAT pathway and MAPK pathway. All the above-mentioned signalling pathways are actively associated with cancers [33–36]. It has been reported that the MAPK signalling pathway played an essential role in the development and aggressive behaviour of tumours by enhancing tumour cell proliferation, differentiation, apoptosis, and cell cycle [37, 38]. Therefore, it is not surprising that the MAPK signalling pathway is involved in HCC tissues. Interestingly, the JAK-STAT pathway was only enriched in the HCC group but not in the AN group. JAK-STAT pathway has been regarded as one of the main molecular pathways in HCC progression [39].

However, the signalling pathway only enriched in the AN group comprised mainly basic metabolisms, such as biological oxidations, amino acids metabolism, TCA cycle, glucose metabolism, and so on. All of these processes belong to the material metabolism and illustrate that the primary material changes play an important role in the tumourigenesis and development of HCC. Also, the different pathways in the HCC and the AN group suggest that there might be different molecular mechanisms in the carcinogenesis and development of the primary HCC in the HCC tissue and the surrounding noncancerous tissues. The above-mentioned results that were analysed demonstrate that our quantitative proteomics approach is suitable in studying the overall molecular profile changes of HCC and could give further insight into the possible molecular mechanisms.

In our study, the proteins in the HCC/DN group could be classified into 3 major clusters: proteins in the red region were related to protein translation and post-translation processing, proteins in the blue region were related to protein glycosylation modification, and proteins in the green region were related to biological metabolic functions dominated by glucose metabolism. As is already known, the malignant proliferation of tumour cells was a process of energy consumption, so the hyperactive glucose metabolism in the HCC group might provide the necessary conditions for the progression of HCC [40, 41]. Glycosylation was involved in the folding, aggregation, maturation, and transportation of protein-peptide chains and was a terminal signal on the surface of the cancer cells in carcinogenesis [42, 43]. The incidence, development, and invasion of HCC were accompanied by glycosylation changes of relevant glycoproteins, so the change of the carbohydrate

structure on the surface of the HCC cells played an important role in the occurrence and development progress of HCC [44, 45].

The proteins in the AN/DN group could also be classified into 3 clusters: the red region represented proteins related to immune and metabolic functions, the green region represented proteins related to apoptosis functions, and the blue region represented proteins related to protein binding functions. This indicated that immune and metabolic changes were relatively active in the para cancer tissues, which might be related to changes in the tumour microenvironment [46–49]. All these results suggest that the evolution of the tissues adjacent to HCC promoted the incidence of HCC.

In summary, this study applied the iTRAQ-based quantitative proteomic approach to analyse the secretome of the primary cultures of HCC tumour tissues. The results visibly showed that the secretome profile alternations and signalling pathways were associated with HCC occurrence and development. The dysregulated proteins in the HCC/DN group were concentrated in the MAPK signalling and JAK-STAT signalling, but the dysregulated proteins in the AN/DN group were more concentrated in the basal material metabolism. The different protein expression profiles in the primary HCC tissues, the surrounding non-cancerous tissues, and the distal noncancerous tissues might also reveal different underlying molecular mechanisms. This study provides a valuable resource of the HCC tissue secretome to investigate the molecular mechanism of HCC incidence and development.

In conclusion, the secretome profile alternations and signalling pathways were associated with HCC incidence and development. The dysregulated proteins in the HCC/DN group were concentrated in the MAPK signalling and JAK-STAT signalling, but the dysregulated proteins in the AN/DN group were more concentrated in the basal material metabolism.

Funding

This work was supported by Key Laboratory of Diagnosis and Treatment of Digestive System Tumors of Zhejiang Province, China (No.2019E10020) and Ningbo Clinical Research Center for Digestive System Tumors, China (No.2019A21003).

Conflict of interest

The authors declare no conflict of interest.

References

1. Ferlay J, Soerjomataram I, Dikshit R, et al. Cancer incidence and mortality worldwide: sources, methods and major patterns in GLOBOCAN 2012. Int J Cancer. 2015; 136: E359-86.
2. Wang FS, Fan JG, Zhang Z, Gao B, Wang HY. The global burden of liver disease: the major impact of China. Hepatology 2014; 60: 2099-108.
3. Sterling RK, Wright EC, Morgan TR, et al. Frequency of elevated hepatocellular carcinoma (HCC) biomarkers in patients with advanced hepatitis C. Am J Gastroenterol 2012; 107: 64-74.
4. Liu X, Cheng Y, Sheng W, et al. Clinicopathologic features and prognostic factors in alpha-fetoprotein-producing gastric cancers: analysis of 104 cases. J Surg Oncol 2010; 102: 249-55.
5. El-Bahrawy M. Alpha-fetoprotein-producing non-germ cell tumours of the female genital tract. Eur J Cancer 2010; 46: 1317-22.
6. Veenstra TD, Conrads TP, Hood BL, Avellino AM, Ellenbogen RG, Morrison RS. Biomarkers: mining the biofluid proteome. Mol Cell Proteomics 2005; 4: 409-18.
7. Anderson NL, Anderson NG. The human plasma proteome: history, character, and diagnostic prospects. Mol Cell Proteomics 2002; 1: 845-67.
8. Hanash SM, Pitteri SJ, Faca VM. Mining the plasma proteome for cancer biomarkers. Nature 2008; 452: 571-9.
9. Paltridge JL, Belle L, Khew-Goodall Y. The secretome in cancer progression. Biochim Biophys Acta 2013; 1834: 2233-41.
10. Slany A, Haudek-Prinz V, Zwickl H, Stättner S, Grasl-Kraupp B, Gerner C. Myofibroblasts are important contributors to human hepatocellular carcinoma: evidence for tumor promotion by proteome profiling. Electrophoresis 2013; 34: 3315-25.
11. Yu Y, Pan X, Ding Y, et al. An iTRAQ based quantitative proteomic strategy to explore novel secreted proteins in metastatic hepatocellular carcinoma cell lines. Analyst 2013; 138: 4505-11.
12. Cao J, Hu Y, Shen C, et al. Nanozeolite-driven approach for enrichment of secretory proteins in human hepatocellular carcinoma cells. Proteomics 2009; 9: 4881-8.
13. Xiao T, Ying W, Li L, et al. An approach to studying lung cancer-related proteins in human blood. Mol Cell Proteomics 2005; 4: 1480-6.
14. Yang L, Rong W, Xiao T, et al. Secretory/releasing proteome-based identification of plasma biomarkers in HBV-associated hepatocellular carcinoma. Sci China Life Sci 2013; 56: 638-46.
15. Zhu J, Warner E, Parikh ND, Lubman DM. Glycoproteomic markers of hepatocellular carcinoma-mass spectrometry based approaches. Mass Spectrom Rev 2019; 38: 265-90.
16. Kim KH, Kim JY, Yoo JS. Mass spectrometry analysis of glycoprotein biomarkers in human blood of hepatocellular carcinoma. Expert Rev Proteomics 2019; 16: 553-68.
17. Zhang J, Liang R, Wei J, et al. Identification of candidate biomarkers in malignant ascites from patients with hepatocellular carcinoma by iTRAQ-based quantitative proteomic analysis. Biomed Res Int 2018; 2018: 5484976.
18. Guo J, Jing R, Zhong JH, et al. Identification of CD14 as a potential biomarker of hepatocellular carcinoma using iTRAQ quantitative proteomics. Oncotarget 2017; 8: 62011-28.
19. Wang Y, Liu H, Liang D, et al. Reveal the molecular signatures of hepatocellular carcinoma with different sizes by iTRAQ based quantitative proteomics. J Proteomics 2017; 150: 230-41.
20. Song C, Ye M, Han G, et al. Reversed-phase-reversed-phase liquid chromatography approach with high orthogonality for multidimensional separation of phosphopeptides. Anal Chem 2010; 82: 53-6.

21. Solaini G, Sgarbi G, Baracca A. Oxidative phosphorylation in cancer cells. Biochim Biophys Acta 2011; 1807: 534-42.
22. Yu M. Somatic mitochondrial DNA mutations in human cancers. Adv Clin Chem 2012; 57: 99-138.
23. Larman TC, DePalma SR, Hadjipanayis AG, et al. Spectrum of somatic mitochondrial mutations in five cancers. Proc Natl Acad Sci USA 2012; 109: 14087-91.
24. Deschênes-Simard X, Lessard F, Gaumont-Leclerc MF, Bardeesy N, Ferbeyre G. Cellular senescence and protein degradation: breaking down cancer. Cell Cycle 2014; 13: 1840-58.
25. Adhikary A, Chakraborty S, Mazumdar M, et al. Inhibition of epithelial to mesenchymal transition by E-cadherin up-regulation via repression of slug transcription and inhibition of E-cadherin degradation: dual role of scaffold/matrix attachment region-binding protein 1 (SMAR1) in breast cancer cells. J Biol Chem 2014; 289: 25431-44.
26. Zhang S, Wang X, Iqbal S, et al. Epidermal growth factor promotes protein degradation of epithelial protein lost in neoplasm (EPLIN), a putative metastasis suppressor, during epithelial-mesenchymal transition. J Biol Chem 2013; 288: 1469-79.
27. Sabit I, Hashimoto N, Matsumoto Y, Yamaji T, Furukawa K, Furukawa K. Binding of a sialic acid-recognizing lectin Siglec-9 modulates adhesion dynamics of cancer cells via calpain-mediated protein degradation. J Biol Chem 2013; 288: 35417-27.
28. Wang F, Weaver VM, Petersen OW, et al. Reciprocal interactions between beta1-integrin and epidermal growth factor receptor in three-dimensional basement membrane breast cultures: a different perspective in epithelial biology. Proc Natl Acad Sci USA 1998; 95: 14821-6.
29. Pikarsky E, Porat RM, Stein I, et al. NF-kappaB functions as a tumour promoter in inflammation-associated cancer. Nature 2004; 431: 461-6.
30. Robichaud N, Hsu BE, Istomine R, et al. Translational control in the tumor microenvironment promotes lung metastasis: phosphorylation of eIF4E in neutrophils. Proc Natl Acad Sci USA 2018; 115: E2202-9.
31. Tahmasebi-Birgani M, Ansari H, Carloni V. Defective mitosis-linked DNA damage response and chromosomal instability in liver cancer. Biochim Biophys Acta Rev Cancer 2019; 1872: 60-5.
32. Yang SF, Chang CW, Wei RJ, Shiue YL, Wang SN, Yeh YT. Involvement of DNA damage response pathways in hepatocellular carcinoma. Biomed Res Int 2014; 2014: 153867.
33. Chang L, Karin M. Mammalian MAP kinase signalling cascades. Nature 2001; 410: 37-40.
34. Burotto M, Chiou VL, Lee JM, Kohn EC. The MAPK pathway across different malignancies: a new perspective. Cancer 2014; 120: 3446-56.
35. Pencik J, Pham HT, Schmoellerl J, et al. JAK-STAT signaling in cancer: from cytokines to non-coding genome. Cytokine 2016; 87: 26-36.
36. Moresi V, Adamo S, Berghella L. The JAK/STAT pathway in skeletal muscle pathophysiology. Front Physiol 2019; 10: 500.
37. Blaj C, Schmidt EM, Lamprecht S, et al. Oncogenic effects of high MAPK activity in colorectal cancer mark progenitor cells and persist irrespective of RAS mutations. Cancer Res 2017; 77: 1763-74.
38. McCubrey JA, Steelman LS, Chappell WH, et al. Roles of the Raf/MEK/ERK pathway in cell growth, malignant transformation and drug resistance. Biochim Biophys Acta 2007; 1773: 1263-84.
39. Vasuri F, Visani M, Acquaviva G, et al. Role of microRNAs in the main molecular pathways of hepatocellular carcinoma. World J Gastroenterol 2018; 24: 2647-60.
40. Noch E, Khalili K. Oncogenic viruses and tumor glucose metabolism: like kids in a candy store. Mol Cancer Ther 2012; 11: 14-23.
41. Grasmann G, Smolle E, Olschewski H, Leithner K. Gluconeogenesis in cancer cells – repurposing of a starvation-induced metabolic pathway? Biochim Biophys Acta Rev Cancer 2019; 1872: 24-36.
42. Rodrigues JG, Balmaña M, Macedo JA, et al. Glycosylation in cancer: selected roles in tumour progression, immune modulation and metastasis. Cell Immunol 2018; 333: 46-57.
43. Cheng WK, Oon CE. How glycosylation aids tumor angiogenesis: an updated review. Biomed Pharmacother 2018; 103: 1246-52.
44. Mehta A, Herrera H, Block T. Glycosylation and liver cancer. Adv Cancer Res 2015; 126: 257-79.
45. Zhang S, Cao X, Gao Q, Liu Y. Protein glycosylation in viral hepatitis-related HCC: characterization of heterogeneity, biological roles, and clinical implications. Cancer Lett 2017; 406: 64-70.
46. Albini A, Bruno A, Noonan DM, Mortara L. Contribution to tumor angiogenesis from innate immune cells within the tumor microenvironment: implications for immunotherapy. Front Immunol 2018; 9: 527.
47. Huang L, Xu H, Peng G. TLR-mediated metabolic reprogramming in the tumor microenvironment: potential novel strategies for cancer immunotherapy. Cell Mol Immunol 2018; 15: 428-37.
48. Reina-Campos M, Shelton PM, Diaz-Meco MT, Moscat J. Metabolic reprogramming of the tumor microenvironment by p62 and its partners. Biochim Biophys Acta Rev Cancer 2018; 1870: 88-95.
49. Jiang X, Wang J, Deng X, et al. Role of the tumor microenvironment in PD-L1/PD-1-mediated tumor immune escape. Mol Cancer 2019; 18: 10.